



# Modelling multivalent defects in thin film solar cells<sup>☆</sup>

Koen Decock<sup>\*</sup>, Samira Khelifi, Marc Burgelman

Department of Electronics and Information Systems (ELIS), University of Gent, St-Pietersnieuwstraat 41, B-9000 Gent, Belgium

## ARTICLE INFO

Available online 17 December 2010

### Keywords:

Solar cells  
Defects in semiconductors  
Computer simulation

## ABSTRACT

Multivalent defects, e.g. double donors/acceptors or amphoteric defects, are important in materials used in solar cell production in general and in chalcopyrite materials in particular. We extended our thin film solar cell simulation software SCAPS to enable the simulation of multivalent defects with up to five different charge states; the algorithms presented are however able to simulate an arbitrary number of possible charge states. The presented solution method avoids numerical inaccuracies caused by the subtraction of two almost equal numbers. This new modelling facility is afterwards used to investigate the consequences of the multivalent character of defects for the simulation of chalcopyrite based solar cells.

© 2010 Elsevier B.V. All rights reserved.

## 1. Introduction

Multivalent defects, i.e. defects with more than two possible charge states are important in several material systems used in solar cell production [1–3]. In particular for chalcopyrite materials, theoretical studies which are in good agreement with measurement results identify most of the existing defects as multivalent defects, e.g. double donors/acceptors [4,5]. The statistics governing this kind of defects differs from the usual Shockley-Read-Hall (SRH) statistics, for defects with only two possible charge states [1].

There exist several numerical simulation tools for thin film solar cells, e.g. AFORS-HET [6], AMPS [7], ASA [3], ASPIN [8], SCAPS [9]. Each of them having specific strengths and weaknesses. As no freely available simulation tool was able up to now to model multivalent defects in their most general form, we extended the recombination facilities of SCAPS. Therefore we developed algorithms which enable the numerical simulation of both the steady state and small signal behaviour of multivalent defects with an arbitrary number of possible charge states. Due to user interface limitations we limited the number of possible charge states to five, which should suffice for most practical problems. These models are afterwards used to demonstrate some differences between the behaviour of a set of SRH-like defects and a multivalent defect.

## 2. Definitions and assumptions

Partially following the notation of Sah and Shockley [1], the different charge states are designated with a subscript  $s$  representing the number

of electrons on the defect. The most positive charge state corresponds then to  $s=0$ , and the most negative to  $s=H$ . The different transitions (defect levels) are designated with a superscript which is the mean value of the charge states involved. For example the density of a defect in state  $s$  is noted as  $N_s$ , and the recombination rate associated with transitions between the states  $s$  and  $s+1$  is noted as  $U^{s+1/2}$ .

The net electron and hole capture rates are noted as  $U_n^{s+1/2}$  and  $U_p^{s+1/2}$  (1).

$$\begin{aligned} U_n^{s+1/2} &= nc_n^{s+1/2} N_s - e_n^{s+1/2} N_{s+1} \\ U_p^{s+1/2} &= pc_p^{s+1/2} N_{s+1} - e_p^{s+1/2} N_s \end{aligned} \quad (1)$$

With  $c_n$  and  $c_p$  the electron and hole capture constants. In order to calculate the emission coefficients ( $e_n$ ,  $e_p$ ) the theory of detailed balance has to be applied. If only two charge states are possible, the occupation probability under thermal equilibrium is given by the Fermi-Dirac distribution. For multivalent defects the grand partition function has to be used instead and take into account possible degeneracies [10,11], leading to the expressions (2),

$$\begin{aligned} e_n^{s+1/2} &= N_c c_n^{s+1/2} \frac{g_s}{g_{s+1}} \exp\left(-\frac{E_C - E_t^{s+1/2}}{kT}\right) \\ e_p^{s+1/2} &= N_v c_p^{s+1/2} \frac{g_{s+1}}{g_s} \exp\left(-\frac{E_t^{s+1/2} - E_V}{kT}\right) \end{aligned} \quad (2)$$

Where  $E_t$  represents the defect level energy level and  $g_s$  represents the degeneracy of the charge state  $s$ . In the common case of a two-level multivalent defect one usually has:  $g_0 = g_2 = g_1/2 = 1$ , which corresponds to an  $s$ -combination out of a two-element set,  $g_s = C_s^2$ . This degeneracy factor can be omitted if the energy level of the defect

<sup>☆</sup> E-MRS Symposium M: V46DB: session M-O12-4 on 11.06.2010 at 09:45.

<sup>\*</sup> Corresponding author. Tel.: +32 9 264 8953.

E-mail address: [Koen.Decock@elis.ugent.be](mailto:Koen.Decock@elis.ugent.be) (K. Decock).

level  $E_t$  is replaced with  $E_t^*$ , which is however temperature dependent (3).

$$E_t^{s+1/2} = E_t^{s+1/2} + kT \ln\left(\frac{g_s}{g_{s+1}}\right) \quad (3)$$

### 3. Numerical procedures and algorithms

In order to calculate the occupation probabilities of the different defect levels continuity has to be expressed (4).

$$\frac{\partial N_s}{\partial t} = U_n^{s-1/2} - U_n^{s+1/2} - U_p^{s-1/2} + U_p^{s+1/2} \quad (4)$$

This expression doesn't hold for the most negative and positive charged states, e.g. for  $s=0$  it should be replaced with (5).

$$\frac{\partial N_0}{\partial t} = -U_n^{1/2} + U_p^{1/2} \quad (5)$$

Expressions (4) and (5) lead to  $H$  independent equations for  $H+1$  unknown variables  $N_s$ . As a last condition, the sum of all defect densities in the different states should be equal to the total defect density  $N_t$ . If the values of the derivatives with respect to time present in (4) are known, this system can be solved. Unfortunately, as one of the charge states usually dominates the others, this system is numerically unstable and should be solved with care, avoiding the subtraction of two almost equal numbers.

#### 3.1. Steady state analysis

In the steady state regime the derivatives with respect to time vanish. Eqs. (4) and (5) are then both reduced to (6).

$$\forall s: U_n^{s+1/2} = U_p^{s+1/2} = U^{s+1/2} \quad (6)$$

Sah and Shockley [1] provide the solution of this system shown in (7) with  $f$  defined in (8).

$$N_s = N_t \frac{f_s}{\sum_{x=0}^H f_x} \quad (7)$$

$$\begin{cases} f_0 = 1 \\ f_s = \prod_{x=0}^{s-1} \frac{nc_n^{x+1/2} + e_p^{x+1/2}}{pc_n^{x+1/2} + e_n^{x+1/2}} \end{cases} \quad (8)$$

The steady state recombination is then given in (9).

$$U^{s+1/2} = (N_s + N_{s+1}) \frac{np c_n^{s+1/2} c_p^{s+1/2} - e_n^{s+1/2} e_p^{s+1/2}}{nc_n^{s+1/2} + pc_p^{s+1/2} + e_n^{s+1/2} + e_p^{s+1/2}} \quad (9)$$

When (9) is expressed in the variables used in SCAPS [12], numerical inaccuracies are avoided and a stable solution is obtained.

#### 3.2. Small signal analysis

In order to be able to simulate the admittance of a solar cell structure, a small signal analysis around the steady state operating point, is carried out in SCAPS [12]. To be able to do this the small signal

values of the occupation probabilities  $\tilde{N}_s$  and the net electron and hole capture rate  $\tilde{U}_n^{s+1/2}$  and  $\tilde{U}_p^{s+1/2}$  (10) are needed.

$$\begin{aligned} \tilde{U}_n^{s+1/2} &= nc_n^{s+1/2} \tilde{N}_s - e_n^{s+1/2} \tilde{N}_{s+1} + c_n^{s+1/2} N_s^{DC} \tilde{n} \\ \tilde{U}_p^{s+1/2} &= pc_p^{s+1/2} \tilde{N}_{s+1} - e_p^{s+1/2} \tilde{N}_s + c_p^{s+1/2} N_{s+1}^{DC} \tilde{p} \end{aligned} \quad (10)$$

$N_s^{DC}$  represents the steady state charge state density and  $\tilde{n}$  and  $\tilde{p}$  are the small signal free carrier densities. The system represented in (4) and (5) again has to be solved, but with the recombination rates replaced by their small signal variants and the sum of all small signal charge state densities equalling zero. The derivatives with respect to time no longer vanish but equal  $j\omega \tilde{N}_s$ . The resulting system unfortunately cannot be solved in the same way as Sah and Shockley solved the system in the steady state regime, and a straightforward solution of the system, e.g. using LU decomposition, is numerically not accurate enough. Hence we propose the following numerically accurate way of solving the system which we implemented in SCAPS. The small signal equivalents of (4) and (5), can be re-expressed as shown in Eq. (11).

$$\tilde{U}_n^{s+1/2} - \tilde{U}_p^{s+1/2} = -j\omega \sum_{x=0}^s \tilde{N}_x \quad (11)$$

Together with (10),  $N_{s+1}$  can be expressed in a recursive way (12). The coefficients are shown in (13) and (14) with  $c_0=1$  and  $d_0=0$ .

$$\tilde{N}_{s+1} = \sum_{x=0}^s a_x \tilde{N}_x + b_s = c_{s+1} \tilde{N}_0 + d_{s+1} \quad (12)$$

$$\begin{aligned} a_{x \neq s} &= \frac{j\omega}{pc_p^{x+1/2} + e_n^{x+1/2}} \\ a_{x=s} &= \frac{j\omega + (nc_n^{x+1/2} + e_p^{x+1/2})}{pc_p^{x+1/2} + e_n^{x+1/2}} \end{aligned} \quad (13)$$

$$\begin{aligned} b_s &= \frac{N_s^{DC} c_n^{s+1/2} \tilde{n} - N_{s+1}^{DC} c_p^{s+1/2} \tilde{p}}{pc_p^{s+1/2} + e_n^{s+1/2}} \\ c_{s+1} &= \sum_{x=0}^s a_x c_x \\ d_{s+1} &= \sum_{x=0}^s a_x d_x + b_s \end{aligned} \quad (14)$$

Expressing the sum of all small signal defect densities to be zero leads to an easy and numerically accurate expression (15).

$$\tilde{N}_s = N_t \frac{\sum_{x=0}^H (c_x d_s - c_s d_x)}{\sum_{x=0}^H c_x} \quad (15)$$

Substituting the first expression of (12) in (10) the small signal recombination rates are calculated in a numerically accurate way as well.

## 4. Results

Consider a multivalent defect with five possible charge states under thermal equilibrium. We simulate the occupation probabilities of the different defect levels as a function of the Fermi level energy. In SCAPS this has been implemented by changing the doping density of the semiconductor material, the results are shown in Fig. 1. As discussed in [1], [10] and [11], the defect is mainly in one charge state unless the Fermi level is close to the defect level energy  $E_t^*$ . The

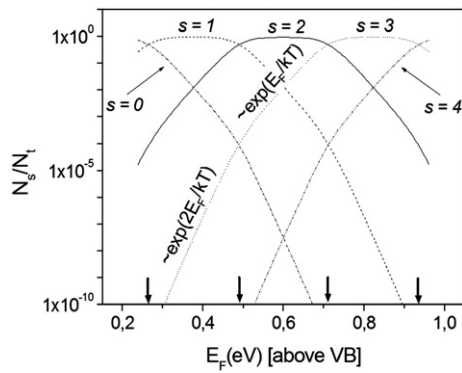


**Fig. 1.** SCAPS simulation of the occupation probabilities of a multivalent defect with five possible charge states under thermal equilibrium conditions. The energy levels corrected with the degeneracy factor (3) of the different defect levels are marked with arrows. The band gap of the material is 1.2 eV.

fraction of defects in a specific charge state falls off exponentially with a slope of an integer times  $1/kT$ .

When the multivalent nature of a defect is not taken into account, it can be modelled as a set of SRH-like defects with energy levels given by  $E_i^*$ . This often leads to good results, but the results are not always consistent. To illustrate the importance of correct multivalent modelling, we start from the ‘NUMOS CIGS baseline.def’ model [13], which is distributed together with the installation package of SCAPS, and which is a good representative for a CIGS thin film solar cell structure. This structure consists of a 3  $\mu\text{m}$  wide CIGS absorber layer, together with a 50 nm CdS buffer layer and a ZnO window layer. In the p-type absorber layer, a band gap of 1.1 eV and a shallow doping density of  $2 \cdot 10^{16} \text{ cm}^{-3}$  is assumed. In this layer, we introduce an amphoteric defect (possible charge states  $-1, 0, +1$ ), with energy levels 0.45 eV and 0.65 eV above the valence band level and with a defect density of  $10^{15} \text{ cm}^{-3}$ , the capture constants are shown in Table 1. The results are compared with the simulation results of the same structure but where the amphoteric defect in the absorber layer has been replaced with a donor defect located at  $0.45 \text{ eV} - kT \ln 2$  and an acceptor defect located at  $0.65 \text{ eV} + kT \ln 2$  above the valence band level, taking into account the degeneracy as shown in Eq. (3). All simulations are performed at 300 K. The results of the simulation of the current-voltage characteristic under AM1.5 illumination conditions are shown in Fig. 2. Taking the defect density of both defects, the same as of the entire amphoteric defect, leads to a bad correspondence of the simulation results and an underestimation of the efficiency by 3.7% absolute. Reducing the defect density however to  $10^{13} \text{ cm}^{-3}$  leads to a good agreement with the simulation results of the amphoteric defect. The results of admittance simulations under dark conditions are shown in Fig. 3. Under thermal equilibrium the simulation results of the structure with the amphoteric defect coincides with the results of the structure with the set of SRH-like defects each having the same defect density as the amphoteric defect. At forward bias voltages the results disagree, especially at low frequencies. Comparing the admittance simulations with the simulations of the structure with a set of SRH-like defects with a decreased defect density, no agreement can be found, even though the current-voltage simulations agreed.

In the structure, there exists a transition of the dominant charge state in the space charge region. With the capture constants chosen as in

**Table 1**  
Overview of the capture constants used for the SCAPS model.

Defect (level)	Donor (+/0)	Acceptor (0/-)
$c_n \text{ (cm}^3/\text{s)}$	$10^{-10}$	$10^{-6}$
$c_p \text{ (cm}^3/\text{s)}$	$10^{-6}$	$10^{-10}$

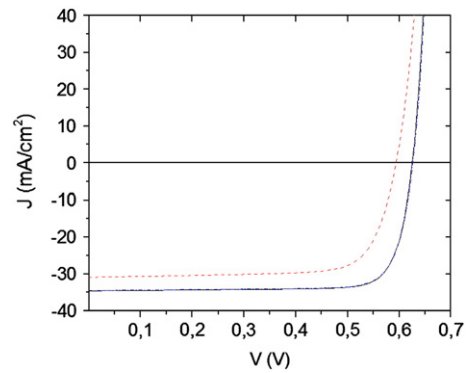


**Fig. 2.** SCAPS simulation of the J-V characteristic under AM1.5 illumination conditions. Comparison of the models with an amphoteric defect (solid line) and an equivalent set of SRH-like defects with the same defect density (dashed line) and with reduced defect density (dash-dotted line). The black solid and blue dash-dotted line coincides. (For interpretation of the references to colour in this figure legend, the reader is referred to the web version of this article.)

Table 1 and under illumination or forward bias voltage, the dominant charge state changes immediately from positive to negative, the neutral charge state is never dominant. It is obvious that this situation cannot be represented by a set of SRH-like defects and hence it leads to different simulation results. The main parameters which trigger this situation are the capture constants and the injection of carriers (through voltage or illumination). Other parameters (temperature, defect density, energetic position of the defect levels) are not determining the existence of the disagreement between the simulations with a multivalent defect and a set of SRH-like defects.

The example above proves that even though some simulations of a structure containing a multivalent defect can be mimicked with a set of SRH-like defects, it is not always possible to find such a model which yields concurring results for different simulations under various conditions. A proper modelling taking into account the true nature of the multivalent defect is thus desirable.

### 5. Conclusions

We extended our thin film solar cell simulation software SCAPS in order to enable the simulation of multivalent defects. Special attention had to be devoted to the numerical stability of the used routines. For the small signal analysis we developed a recursive solution method which avoids numerical inaccuracies.

This new facility was afterwards used to demonstrate that ignoring the multivalent nature of a defect and modelling it as a set of SRH-like defects can have an important influence on the simulation results.

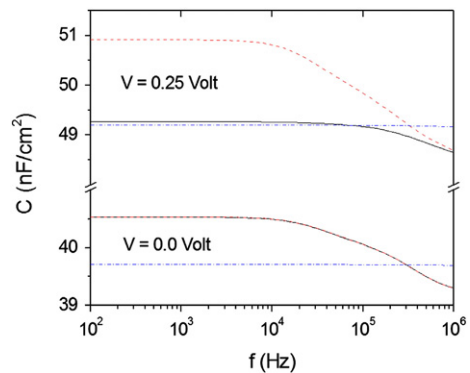


**Fig. 3.** SCAPS simulation of the capacitance as a function of the frequency under dark conditions, and different bias voltages  $V$ . Comparison of the models with an amphoteric defect (solid lines) and an equivalent set of SRH-like defects with the same defect density (dashed lines) and with reduced defect density (dash-dotted lines). At  $V = 0.0 \text{ V}$  the solid and the dashed line coincide.

## Acknowledgements

We acknowledge the support of the Research Foundation—Flanders (K.D., Ph.D. Fellowship).

## References

- [1] C.-T. Sah, W. Shockley, *Phys. Rev.* 109 (4) (1958) 1103.
- [2] A. Milnes, *Deep Impurities in Semiconductors*, John Wiley and sons, New York, 1973.
- [3] R.E.I. Schropp, M. Zeman, *Amorphous and Microcrystalline Silicon Solar cells*, Kluwer academic publishers, Norwell, 1998.
- [4] S. Siebentritt, U. Rau, *Wide-Gap Chalcopyrites*, Springer-Verlag, Berlin Heidelberg, 2006.
- [5] S.B. Zhang, S.H. Wei, A. Zunger, *Phys. Rev. B* 57 (16) (1997) 9642.
- [6] A. Froitzheim, R. Stangl, M. Krieger, L. Elstner, W. Fuhs, *Proceedings of the 3rd World conference on Photovoltaic Solar Energy Conversion, Osaka (J)*, 2003, 1P-D3-34.
- [7] Developed at Pennsylvania State University under the direction of S.J.Fonash, see: <http://www.ampsmodeling.org/default.htm> (last accessed July 2010).
- [8] F. Smole, J. Krč, J. Furlan, *Sol. Energy Mater. Sol. Cells* 34 (1994) 385.
- [9] M. Burgelman, P. Nollet, S. Degrave, *Thin Solid Films* 361–362 (2000) 527.
- [10] D.C. Look, *Phys. Rev. B* 24 (10) (1981) 5852.
- [11] W. Shockley, J.T. Last, *Phys. Rev.* 107 (2) (1957) 392.
- [12] A. Niemegeers, S. Gillis, M. Burgelman, in: J. Schmid, H.A. Ossenbrink, P. Helm, H. Ehmman, E.D. Dunlop (Eds.), *Proceedings of the 2nd World conference on Photovoltaic Solar Energy Conversion, Vienna (A)*, 1998, p.672.
- [13] M. Burgelman, J. Verschraegen, B. Minnaert, J. Marlein, in M. Burgelman, M. Topič (Eds.), *Proceedings of NUMOS, Gent, B.*, 2007, p.357.